

ULRR

Design and piezoelectric energy harvesting properties of a ferroelectric cyclophosphazene salt

Item Type	Article
Authors	Deswal, Swati;Panday, Rishukumar;Naphade, Dipti R.;Cazade, Pierre-Andre;Guerin, Sarah;Zareba, Jan K.;Steiner, Alexander;Ogale, Satishchandra;Anthopoulos, Thomas D.;Boomishankar, Ramamoorthy
Citation	Small, 2023, 2300792
Publisher	Wiley and Sons Ltd
Download date	2026-06-16 05:52:35
Item License	https://creativecommons.org/licenses/by-nc-sa/4.0/
Link to Item	https://doi.org/10.34961/researchrepository-ul.23790888

Design and Piezoelectric Energy Harvesting Properties of a Ferroelectric Cyclophosphazene Salt

Swati Deswal, Rishukumar Panday, Dipti R. Naphade, Pierre-Andre Cazade, Sarah Guerin,* Jan K. Zaręba,* Alexander Steiner,* Satishchandra Ogale,* Thomas D. Anthopoulos,* and Ramamoorthy Boomishankar*

Cyclophosphazenes offer a robust and easily modifiable platform for a diverse range of functional systems that have found applications in a wide variety of areas. Herein, for the first time, it reports an organophosphazene-based supramolecular ferroelectric [(PhCH₂NH)₆P₃N₃Me]I, [PMe]I. The compound crystallizes in the polar space group *Pc* and its thin-film sample exhibits remnant polarization of 5 $\mu\text{C cm}^{-2}$. Vector piezoresponse force microscopy (PFM) measurements indicated the presence of multiaxial polarization. Subsequently, flexible composites of [PMe]I are fabricated for piezoelectric energy harvesting applications using thermoplastic polyurethane (TPU) as the matrix. The highest open-circuit voltages of 13.7 V and the maximum power density of 34.60 $\mu\text{W cm}^{-2}$ are recorded for the poled 20 wt.% [PMe]I/TPU device. To understand the molecular origins of the high performance of [PMe]I-based mechanical energy harvesting devices, piezoelectric charge tensor values are obtained from DFT calculations of the single crystal structure. These indicate that the mechanical stress-induced distortions in the [PMe]I crystals are facilitated by the high flexibility of the layered supramolecular assembly.

1. Introduction

Ever since the discovery of ferroelectricity in Rochelle salt (KNaC₄H₄O₆·4H₂O) and potassium dihydrogenphosphate (KH₂PO₄), ferroelectrics have become a burgeoning class of functional materials.^[1,2] They are employed as ferroelectric random-access memories, capacitors, sensors, actuators, electromechanical transducers, field-effect transistors, efficient photovoltaics, and as mechanical energy harvesters.^[3–6] While inorganic oxides dominated the commercial market for decades, growing environmental concerns have driven technological interest in small-molecule-based ferroelectrics.^[7–11] Aided by non-covalent interactions, supramolecular chemistry offers a versatile platform for designing new ferroelectric materials with desired functionalities and improved charge polarization characteristics.^[12–14] Several two-component systems containing acyclic cations such as ammonium and

S. Deswal, R. Panday, R. Boomishankar
Department of Chemistry and Centre for Energy Science
Indian Institute of Science Education and Research, Pune
Dr. Homi Bhabha Road, Pune 411008, India
E-mail: boomi@iiserpune.ac.in

D. R. Naphade, T. D. Anthopoulos
King Abdullah University of Science and Technology (KAUST)
KAUST Solar Center (KSC)
Thuwal 23955–6900, Saudi Arabia
E-mail: thomas.anthopoulos@kaust.edu.sa


P.-A. Cazade, S. Guerin
Department of Physics
Bernal Institute
University of Limerick
Limerick V94 T9PX, Ireland
E-mail: Sarah.Guerin@ul.ie

J. K. Zaręba
Institute of Advanced Materials
Faculty of Chemistry
Wroclaw University of Science and Technology
Wroclaw 50- 370, Poland
E-mail: Jan.Zareba@pwr.edu.pl

A. Steiner
Department of Chemistry
University of Liverpool
Crown Street, Liverpool L69 7ZD, UK
E-mail: a.steiner@liverpool.ac.uk

S. Ogale
Department of Physics and Centre for Energy Science
Indian Institute of Science Education and Research, Pune
Dr. Homi Bhabha Road, Pune 411008, India
E-mail: satishogale@iiserpune.ac.in

S. Ogale
Research Institute for Sustainable Energy (RISE)
TCG Centres for Research and Education in Science and Technology
(TCG-CREST)
Salt Lake, Kolkata 700091, India

 The ORCID identification number(s) for the author(s) of this article can be found under <https://doi.org/10.1002/small.202300792>

© 2023 The Authors. Small published by Wiley-VCH GmbH. This is an open access article under the terms of the Creative Commons Attribution License, which permits use, distribution and reproduction in any medium, provided the original work is properly cited.

DOI: 10.1002/small.202300792

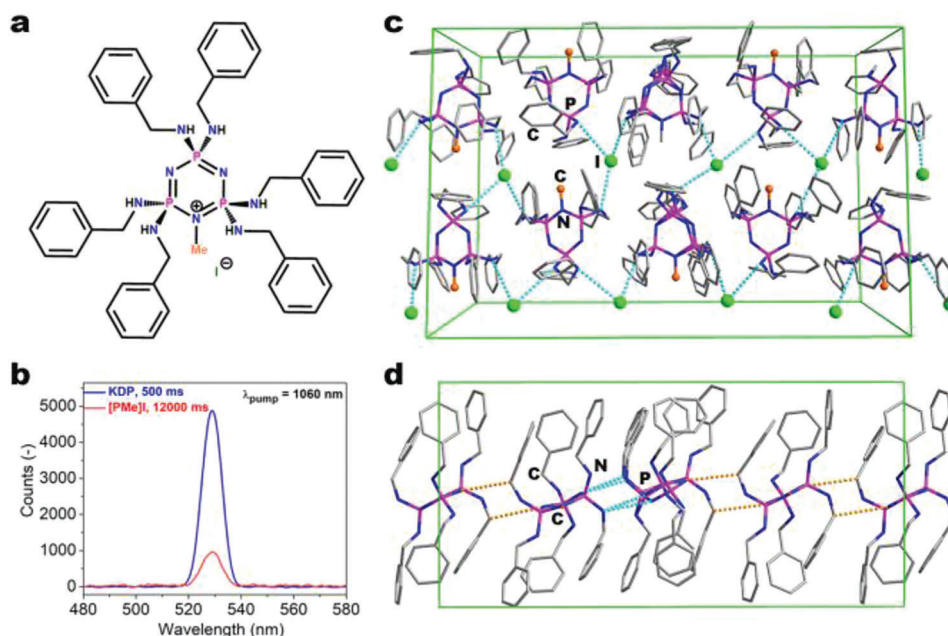


Figure 1. a) Schematic diagram of [PMe]I. b) SHG plot of [PMe]I. c) Crystal structure showing the 2D hydrogen-bonded network connected via NH...I interactions. d) Ribbons of [PMe]⁺ ions mediated by NH...N and CH...N contacts.

phosphonium ions or cyclic cations such as DABCO (1,4-diazabicyclo[2.2.2]octane), TCM (trimethyl chloromethyl ammonium), EDABCO (N-ethyl-1,4-diazoniabicyclo[2.2.2]octonium), pyrrolidinium and quinuclidinium ions, etc. have been investigated in combination with mono- and polyatomic anions.^[11,15–18] However, many of these systems suffer from low polarization values or Curie points (T_C) near or below room temperature, which is limiting their applications. Cyclophosphazenes are a versatile class of inorganic ring systems. Their ring backbone of alternating phosphorus and nitrogen atoms is chemically highly inert offering a robust platform for anchoring a wide variety of substituents. This has led to a myriad of functionalized systems that have been explored as antibacterial agents, heterogeneous catalysts, sensors, biomedical materials, and flame retardants to name a few.^[19–25] The commercially available precursor hexachlorocyclotriphosphazene (cyclo- $P_3N_3Cl_6$) has six chlorine atoms that are readily replaced by nucleophiles such as amino groups.^[26] Furthermore, the N-ring sites of amino-phosphazenes can be alkylated to yield N-alkylphosphazanium ions.^[27] Inspired by their great scope for modification and ability to self-assemble into crystalline supramolecular arrays,^[25–28] we envisioned that phosphazanium salts could also serve as ferroelectric materials.

Herein, we report for the first time the utilization of a cyclotriphosphazene as a ferroelectric material, in the form of its two-component ionic system, [(PhCH₂NH)₆P₃N₃Me]I ([PMe]I). Ferroelectric measurements of this material gave a remnant polarization (P_r) value of 5 $\mu\text{C cm}^{-2}$. The ferroelectric domain structure of [PMe]I has been visualized by vector PFM measurements. Furthermore, a thermoplastic polyurethane (TPU) composite of [PMe]I was tested for piezoelectric energy harvesting applications. The maximum output voltage of 13.7 V and the power density value of 34.60 $\mu\text{W cm}^{-2}$ were recorded for the poled

20 wt.% [PMe]I/TPU device. The DFT calculations on [PMe]I crystals show a maximum strain constant of 25 pC N⁻¹, which is responsible for its efficient nanogenerator attributes.

2. Results and Discussion

The organic phosphazene salt [(PhCH₂NH)₆P₃N₃Me]I, [PMe]I, (Figure 1a) was synthesized by the reaction of the benzyl amino derivative P₃N₃(PhCH₂NH)₆, (P) with methyl iodide (Scheme S1, Supporting Information). The compound melts at 185 °C and decomposes above 253 °C as indicated by thermogravimetric analysis (Figure S7, Supporting Information). Colorless crystals of [PMe]I were obtained from the slow evaporation of a solution in methanol at room temperature. Single crystal X-ray diffraction (SCXRD) analysis revealed that the compound crystallizes in the polar monoclinic space group *Pc* (Table S1, Supporting Information). The non-centrosymmetric nature of [PMe]I was further confirmed by the detection of a second harmonic generation (SHG) signal for the powdered sample upon irradiation with 1060 nm femtosecond laser pulses at 293 K, with a relative SHG efficiency of ca. 0.01 versus potassium dihydrogenphosphate (KDP) (Figure 1b).

The low-temperature structure that was measured at 120 K is very similar to that recorded at room temperature (see Figures S3 and S4, Supporting Information for crystallographic data). The asymmetric unit of [PMe]I contains four N-methylphosphazanium cations and four iodide anions. The bond lengths and angles of the P₃N₃ ring are consistent with structural parameters found in other N-alkylphosphazanium salts.^[27] Similar to phosphazanium rings in structures reported previously, the rings in [PMe]I is slightly puckered. One of the four crystallographically independent rings shows an out-of-plane disorder that could be resolved for the low-temperature data (120 K)

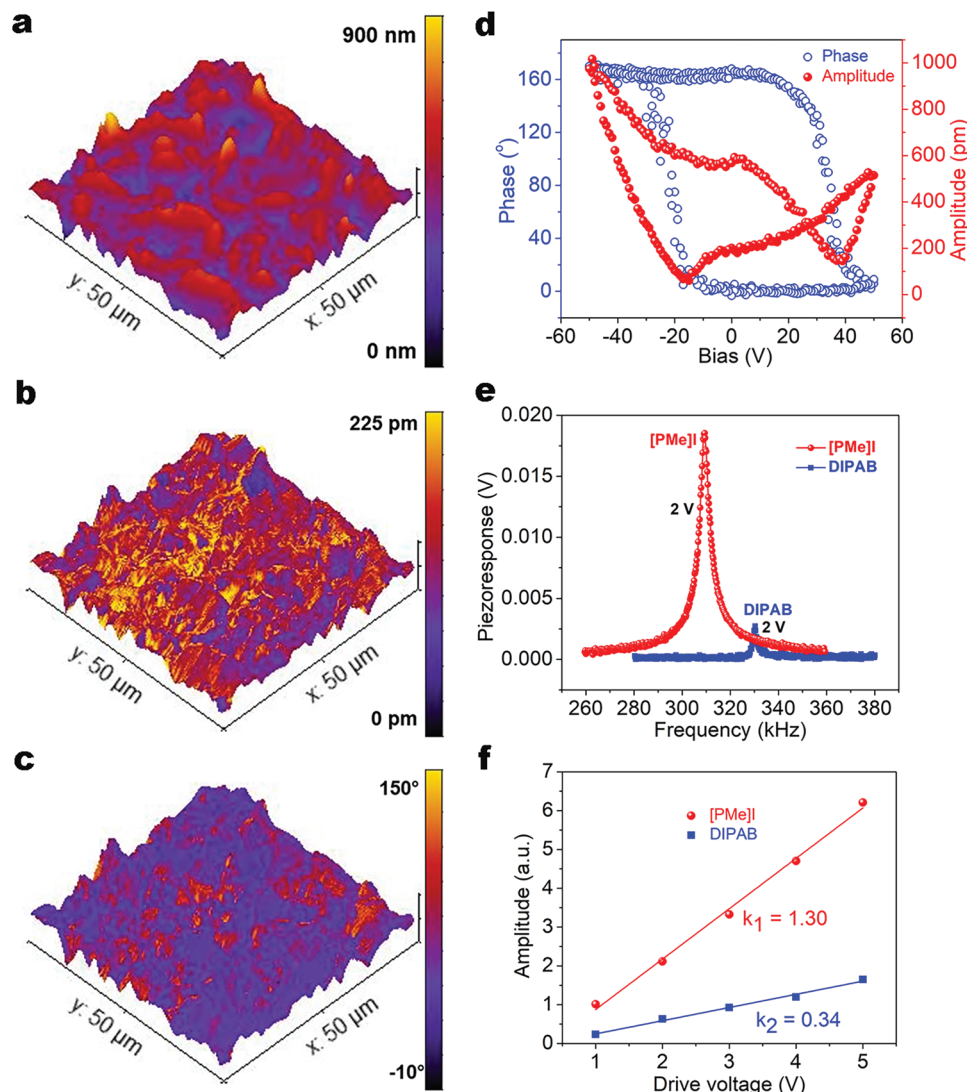


Figure 2. a–d) Diagram representing vector PFM images showing a) 3D-topography, b) 3D-vertical amplitude, c) 3D-vertical phase, and d) local PFM phase versus bias and amplitude versus bias hysteresis loop for a selected point on the thin film. e) Comparative PFM resonance curves of [PMe]I and DIPAB at 2 V. f) Pointwise amplitude versus drive voltage measurements on [PMe]I and DIPAB crystal surface.

but masked at room temperature by the somewhat larger thermal displacement parameters (Figure S5, Supporting Information). In the crystal, [PMe]I forms a layered structure. The shortest contacts between [PMe]⁺ and I[−] ions are NH...I interactions resulting a 2D hydrogen-bonded network (Figure 1c). Within this network, the [PMe]⁺ ions are arranged in ribbons mediated by NH–N(ring) and CH–N(ring) contacts that involve the amino and the methylene groups of the benzylamino substituents (Figure 1d).

It is noteworthy that only two of the four crystallographically independent [PMe]⁺ ions are engaged in NH–N bonds, which underlines the low symmetry of the structure. The central realm of heteroatoms is sandwiched between hydrophobic domains of peripheral benzyl groups that interact with each other mainly via CH– π contacts. The arrangement is reminiscent to that of lipid bilayers. The bulk phase purity of [PMe]I was established by powder X-ray diffraction (PXRD) measurements (Figure S6, Supporting

Information). Differential scanning calorimetry measurements of [PMe]I confirmed the absence of any phase transition up to the melting point (Figures S8–S10, Supporting Information).

To elucidate the domain structure and polarization switching behavior of [PMe]I, we performed Piezoresponse Force Microscopy (PFM) studies. Vector mode, vertical (V), and lateral (L), PFM studies were conducted to measure the respective out-of-plane and in-plane piezoelectric signals. **Figure 2a** illustrates the 3D topography and Figures 2b,c represents the corresponding V-PFM amplitude and phase mappings overlaid on the topography. The bright and dark contrasts in the amplitude image reflect the magnitude of the piezoresponse and the color difference in the phase image (Figure 2c) reveals polarization orientation for each domain. The V-PFM and L-PFM results show differences in the domain size and structure within the individual [PMe]I flake (Figure S12, Supporting Information). The strong vector amplitude signals (both lateral and vertical) and the presence of

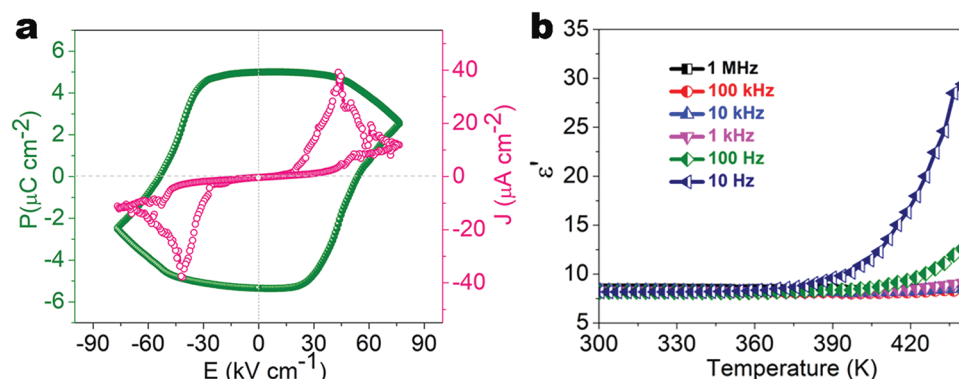


Figure 3. a) P-E hysteresis loop and leakage current density plot of [PMeI] on a drop-casted film. b) The temperature-dependent real part of dielectric permittivity (ϵ') of [PMeI] at various frequencies.

non-180° domain walls support the multiaxial nature of [PMeI] showing domains with diverse polarization orientations.^[29] Similar observations have also been made from the V-PFM images on a single crystal of [PMeI] (Figure S13, Supporting Information). The PFM spectroscopy performed on a single point of the thin film gave a well-defined hysteresis phase loop and a butterfly-shaped amplitude loop (Figure 2d). The phase change by 180° implies a complete polarization switching behavior in the sample.

Furthermore, the obtained PFM resonance curve at 2 V on the [PMeI] surface showed a higher peak value than that of the standard sample of diisopropyl ammonium bromide (DI-PAB) confirming the excellent piezoelectric nature of [PMeI] (Figure 2e).^[30] Subsequently, the pointwise Amplitude versus drive voltage measurements were performed on the ferroelectric domains of both [PMeI] and DIPAB (Figure 2f). The linearity of the amplitude data as a function of driving voltage suggests the intrinsic piezoelectric nature of both [PMeI] and DIPAB. Notably, the relative magnitude of the piezoelectric coefficient of [PMeI], determined from the ratio of the slopes of these fitted lines, is approximately four times higher than that of DIPAB crystal.

The ferroelectric nature of [PMeI] was further established by performing polarization versus electric field (*P-E*) measurements on its thin film sample using the Sawyer-Tower Circuit. The measurements manifested a well-resolved rectangular hysteresis loop at an operating frequency of 0.03 Hz (Figure 3a). A reasonably good remnant polarization value of 5 $\mu\text{C cm}^{-2}$ was obtained at 298 K. The obtained value is comparable with the polarizations reported for various other emerging organic molecular ferroelectric materials.^[31,32] The leakage current density plots of [PMeI] measured along the *P-E* loop exhibit two opposite peaks, signifying two stable states of opposite polarizations and thereby supporting the ferroelectric nature of the obtained loops. The observation of slightly higher leakage currents could presumably be attributed to the presence of grain boundaries in the thin film sample of [PMeI] and the resistance from the electrical circuits due to the high electric fields.^[33] Temperature-dependent polarization (%) measurement has been performed on the 8 mm diameter and 0.98 mm thick pellet of [PMeI] by applying 100 V bias voltage at an operating frequency of 100 Hz. This measurement also revealed an increase in polarization at higher temperatures and the absence of any phase transition (Figure S14, Supporting In-

formation). Furthermore, temperature-dependent dielectric permittivity measurements on compacted pellet show no apparent dielectric anomalies in [PMeI] (Figures 3b; Figures S15–S17, Supporting Information), confirming the absence of any structural phase transitions from RT up to 440K. The probable reason for the absence of phase transitions in [PMeI] could be the bulkiness of substituents attached to the phosphazanium cation. However, a significant rise in the ϵ' values is witnessed above 360 K, which stems from more polarizable domains and enhanced ionic conductivity in the compound closer to its melting point. A maximum ϵ' value of 8.2 was obtained at room temperature for [PMeI] at 1 kHz. Moreover, the compound displays considerably low dielectric loss factors ($\tan \delta$) as observed from its electrical energy dissipation, which mirrors the observed trends in the ϵ' versus temperature plot (Figure S15, Supporting Information). Similar trends were observed from frequency-dependent ϵ' and $\tan \delta$ plots with varying temperatures (Figures S15–S17, Supporting Information).

The polarization switching is facilitated by the flexibility of the supramolecular assembly. However, due to the complex nature of the crystal structure containing four independent ion pairs, it is difficult to identify a specific moiety being solely responsible for this effect. Possible causes could be (a) the shifting of iodide ions, which show anisotropic displacement parallel to the hydrogen-bonded network and (b) the phosphazene rings, which could flip between puckered conformers. An indication of this is the out-of-plane disorder of one of the rings.

Propelled by the excellent ferroelectric properties of [PMeI], we explored its utility for piezoelectric energy harvesting applications. For these studies, polymer composites with varying weight percentages (wt.%) were prepared by dissolving suitable quantities of [PMeI] into homogeneous solutions containing thermoplastic polyurethane (TPU) in THF. All formulated composites exhibited excellent mechanical flexibility (Figures 4a; Figure S18 and Table S4, Supporting Information).

The PXRD of the composite films showed a rise in the PXRD reflection intensities upon increasing the loading of the ferroelectric crystallites in the composite films (Figure S19b, Supporting Information). At the lower concentrations, the [PMeI] crystallites orient primarily along the *a*-direction (planes (1 0 0), (2 0 0), and (3 0 0), (Figure S19b, Supporting Information)). However, at higher concentrations (25 wt.%) additional peaks start to

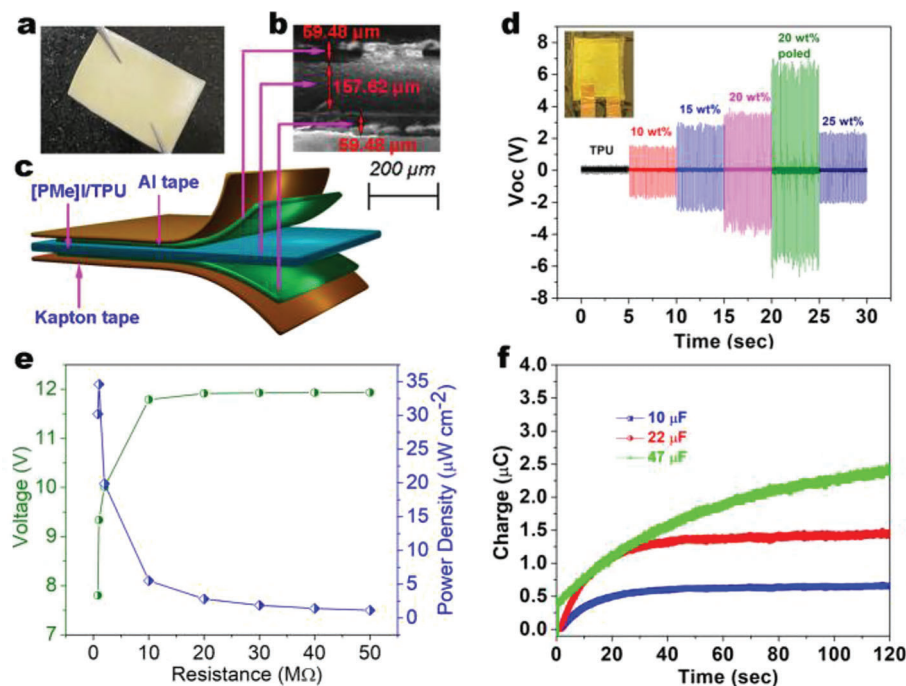


Figure 4. a) Photograph of the 20 wt.% [PMeI]/TPU composite film under stretching operation. b) Cross-sectional SEM image of [PMeI]/TPU and c) the schematic diagram of the composite device d) Comparative output voltage performance of all wt.% [PMeI]/TPU composite devices with a shifted time axis. e) Voltage and power density plots as a function of load resistance corresponding to the poled 20 wt.% [PMeI]/TPU device. f) Plots of accumulated charges for different rated capacitors were obtained by employing the poled 20 wt.% [PMeI]/TPU.

appear due to agglomeration. The peak at 19.9° in the 25 wt.% [PMeI]/TPU composite corresponds to the (0 6 2) plane, which suggests the random orientation of the crystallites in this composite. The surface morphologies probed by scanning electron microscopy (SEM) indicated the random distribution of the [PMeI] crystallites in the polymer matrix (Figure S20, Supporting Information). Based on the cross-sectional SEM image, the thickness of the composite film, sandwiched between the Al electrodes, was calculated to be 0.15 mm (Figure 4b).

Piezoelectric energy harvesting experiments were performed by applying a periodic compressive force directly on the as-prepared devices using a home-built vertical impact setup coupled with an oscilloscope. The open-circuit voltages (V_{oc}) were recorded under an applied force of 21 N at a frequency of 9 Hz as optimized from the previous studies (Figure S22a, Supporting Information). The measured V_{oc} exhibits a strong correlation with the concentration of the ferroelectric particles present in the composite. When the particle concentration increases from 10 wt.% to 20 wt.% in the [PMeI]/TPU composites, the V_{oc} increases from 3.4 to 7.7 V (Figure 4d). The noteworthy improvement in the output performances of the devices can be attributed to the enhanced piezoelectric response of the composites, which stems from Maxwell-Sillars polarization developing at the interfaces between the ferroelectric fillers and the bulk polymer.^[34,35] When the force is applied to the device, the free electrons from electrodes move back and forth to nullify the piezoelectric potential generated from the impact. Subsequently, an alternating voltage is generated in an external circuit to counter the flow of electrons from both electrodes into the circuit. The lower performance of the 25 wt.% composite is attributed to the agglomeration of the

ferroelectric crystallites, which hinders the alignment of electric dipoles at a longer range, thereby weakening the electromechanical coupling effect (Figure S21, Supporting Information). Importantly, the performance of the optimal 20 wt.% [PMeI]/TPU was found to improve upon subjecting the device to poling (25 kV for 2 h at 298 K), which results in a much higher V_{oc} of 13.7 V at the optimized force of 21 N and 9 Hz frequency (S22b, Supporting Information).

The output characteristics of the best-performing poled 20 wt.% device was further evaluated over a wide range of load resistances ranging from 0.8 to 50 M Ω . The output voltage increases sharply and then saturates with increasing resistance. (Figure 4e). A maximum power density (PD) value of $34.60 \mu\text{W cm}^{-2}$ was recorded at an optimal load of 1 M Ω for the device based on poled 20 wt.% [PMeI]/TPU (Figure 4e; Figure S24, Supporting information). Furthermore, mechanical durability tests performed on the optimized poled 20 wt.% [PMeI]/TPU device reveal no degradation in signal amplitude even after 2500 cycles of continuous impact (Figure S23, Supporting Information).

To demonstrate the practical utility, the electricity generated from the poled [PMeI]/TPU device was directly applied to charge aluminum capacitors using a full-wave bridge rectifier. As observed from the charging curves, the poled 20 wt.% [PMeI]/TPU champion device was found to charge the 10, 22, and 47 μF capacitors within 120 s with the maximum accumulated charges of 0.66, 1.39, and 2.42 μC , and stored electrical energies of 0.022, 0.043, and 0.063 μJ , respectively (Figures 4f; Figure S25, Supporting Information). These results promise their utility in low-power electronic circuits and systems.

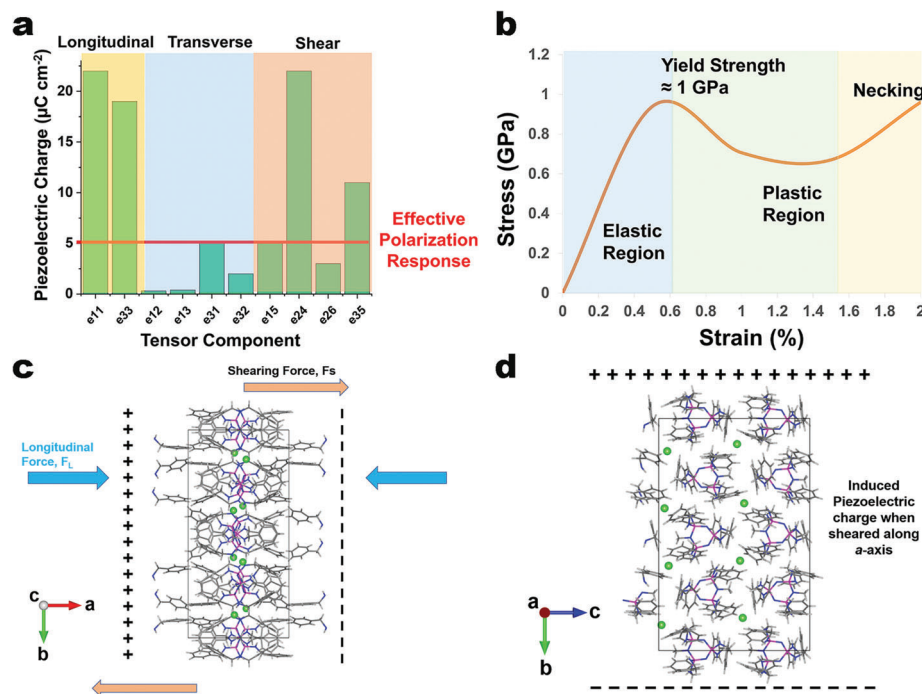


Figure 5. a) DFT-calculated piezoelectric charge tensor values for a [PMe]I unit cell. Longitudinal values are shaded in yellow, transverse in blue, and shear in orange. b) The *in-silico* calculated stress-strain curve of the [PMe]I single crystal. c,d) DFT-optimized [PMe]I single crystal showing the applied forces that induce the highest indicated piezoelectric polarization. c) Squeezing and bending along the *a*-axis will induce a polarization of $22 \mu\text{C cm}^{-2}$. Squeezing includes dipoles along the *a*-axis, d) whilst bending induces dipoles along the *b*-axis.

To understand the device performance at the atomic scale, Density Functional Theory (DFT) calculations were carried out on the [PMe]I single crystal. The monoclinic space group allows for ten (two longitudinal, four transverse, and four shear) non-zero piezoelectric components (Figure 5a). The predicted piezoelectric charge tensor values representing the induced polarization along a specific crystallographic axis, range from 0.3 – $22 \mu\text{C cm}^{-2}$. This observation is in line with the average polarization of $5 \mu\text{C cm}^{-2}$ measured for [PMe]I with random orientation of the crystallites. Both e_{31} and e_{15} are predicted to have polarization values of $5 \mu\text{C cm}^{-2}$ (red line, Figure 5a). The highest predicted piezoelectric constants are e_{11} and e_{24} with charge values of $22 \mu\text{C cm}^{-2}$, followed by an e_{33} value of $19 \mu\text{C cm}^{-2}$. The high e_{11} value corresponds to the crystallographic *a*-axis, which is perpendicular to the plane of P-N rings. The high e_{24} value indicates that applying a shearing force along the *a*-axis will induce a large piezoelectric dipole in the perpendicular *b*-axis. A dipole along the *b*-axis would run parallel to the hydrogen-bonded network. Figures 5c,d shows these responses as a function of the supramolecular packing in the [PMe]I crystal. These results indicate that crystal distortions that reduce the distance between neighboring iodide ions result in the largest induced charge.

When strained along the crystallographic *c*-axis, the crystal is predicted to have a mechanical stiffness of 2 GPa (Figure 5b). The [PMe]I system reaches its ultimate tensile strength at very low strain values, which suggests that the crystals would be brittle if not reinforced by the TPU. The poor mechanical stiffness of the [PMe]I crystals is evident from its direct piezoelectric charge coefficient (d_{33}) value of 0.13 pC/N , obtained from the Berlincourt

method. The measured high voltage output is reflected in the calculated dielectric permittivity of 2.8. Combining these values with the average device polarization values of $5 \mu\text{C cm}^{-2}$ yields the piezoelectric strain and voltage constants of 25 pC N^{-1} and 1 V mN^{-1} , respectively.

3. Conclusions

In summary, a newly designed two-component ferroelectric [PMe]I consisting of N-methyl phosphazanium cations and iodide ions was synthesized and utilized for piezoelectric energy harvesting applications. The compound crystallized in polar space group *Pc*; the ferroelectric measurements on its thin-film sample displayed a remnant polarization value of $5 \mu\text{C cm}^{-2}$. Vector PFM studies reveal the presence of spherulitic domain structures and multiaxial polarization in [PMe]I. Moreover, its potential application for energy harvesting devices was studied in the form of TPU composites. A maximum V_{oc} of 13.7 V and the highest power density of $34.60 \mu\text{W cm}^{-2}$ was obtained from poled 20 wt.% [PMe]I/TPU composite. The electricity generated was subsequently utilized to charge an external capacitor which further illustrates the tremendous potential of these novel supramolecular ferroelectrics for use in self-powered electronics. The effective nanogenerator performance of these composite devices was attributed to the high piezoelectric strain constant of 25 pC N^{-1} as revealed by the DFT analysis of [PMe]I crystal. Organophosphazenes are versatile synthons, and this study unfolds a hitherto unknown application for this class of compounds in non-linear dielectrics.

Supporting Information

Supporting Information is available from the Wiley Online Library or from the author.

Acknowledgements

S.D., R.P. contributed equally to this work. This work was supported by SERB, India via Grant no. CRG/2019/004615 (R.B.). R.B. thanks SERB-STAR via Grant no. STR/2021/000016. T.D.A. and D.R.N. were grateful to KAUST and KSC for the financial support. P.A.C. and S.G. acknowledge the support from the Irish Centre for High-End Computing (ICHEC) and Science Foundation Ireland (12/RC/2275_P2). S.G. acknowledges support from the Science Foundation Ireland (21/PATH-S/9737) and the European Union (101039636). The views and opinions expressed were, however, those of the author only and did not necessarily reflect those of the European Union or the European Research Council. Neither the European Union nor the granting authority can be held responsible. J.K.Z. acknowledges support from Academia Iuvenum, Wrocław University of Science and Technology. The authors thank P. Dixit and Dr. B. Praveenkumar for polishing the composite devices.

Open access funding provided by IReL.

Conflict of Interest

The authors declare no conflict of interest.

Data Availability Statement

The data that support the findings of this study are available in the supplementary material of this article.

Keywords

cyclophosphazene, energy harvester, ferroelectric, piezoelectric, piezoresponse force microscopy

Received: January 30, 2023

Revised: July 3, 2023

Published online:

- [1] J. Valasek, *Phys. Rev.* **1921**, 17, 475.
- [2] G. Busch, P. Scherrer, *Naturwissenschaften* **1935**, 23, 737.
- [3] J. Scott, *Science* **2007**, 315, 954.
- [4] S. Yang, J. Seidel, S. Byrnes, P. Shafer, C.-H. Yang, M. Rossell, P. Yu, Y.-H. Chu, J. Scott, J. Ager, *Nat. Nanotechnol.* **2010**, 5, 143.
- [5] J. Hoffman, X. Pan, J. W. Reiner, F. J. Walker, J. Han, C. H. Ahn, T. Ma, *Adv. Mater.* **2010**, 22, 2957.
- [6] C. Bowen, H. Kim, P. Weaver, S. Dunn, *Energy Environ. Sci.* **2014**, 7, 25.
- [7] G. H. Haertling, *J. Am. Ceram. Soc.* **1999**, 82, 797.
- [8] D. J. Goossens, *Acc. Chem. Res.* **2013**, 46, 2597.
- [9] W. Zhang, R.-G. Xiong, *Chem. Rev.* **2012**, 112, 1163.
- [10] W. Li, Z. Wang, F. Deschler, S. Gao, R. H. Friend, A. K. Cheetham, *Nat. Rev. Mater.* **2017**, 2, 16099.
- [11] H.-Y. Zhang, Y.-Y. Tang, P.-P. Shi, R.-G. Xiong, *Acc. Chem. Res.* **2019**, 52, 1928.
- [12] A. S. Tayi, A. Kaeser, M. Matsumoto, T. Aida, S. I. Stupp, *Nat. Chem.* **2015**, 7, 281.
- [13] R. Kumai, S. Horiuchi, H. Sagayama, T.-h. Arima, M. Watanabe, Y. Noda, Y. Tokura, *J. Am. Chem. Soc.* **2007**, 129, 12920.
- [14] S. Horiuchi, R. Kumai, Y. Tokura, *J. Am. Chem. Soc.* **2013**, 135, 4492.
- [15] Y.-M. You, W.-Q. Liao, D. Zhao, H.-Y. Ye, Y. Zhang, Q. Zhou, X. Niu, J. Wang, P.-F. Li, D.-W. Fu, *Science* **2017**, 357, 306.
- [16] G. Huang, A. A. Khan, M. M. Rana, C. Xu, S. Xu, R. Saritas, S. Zhang, E. Abdel-Rahmand, P. Turban, S. Ababou-Girard, *ACS Energy Lett.* **2020**, 6, 16.
- [17] S. Wang, A. A. Khan, S. Teale, J. Xu, D. H. Parmar, R. Zhao, L. Grater, P. Serles, Y. Zou, T. Filleter, *Nat. Commun.* **2023**, 14, 1852.
- [18] T. Vijayakanth, F. Ram, B. Praveenkumar, K. Shanmuganathan, R. Boomishankar, *Angew. Chem., Int. Ed.* **2020**, 59, 10368.
- [19] X. Su, L. Wang, J. Xie, X. Liu, H. Tomás, *Curr. Org. Chem.* **2021**, 25, 301.
- [20] S. Yang, Y. Zhu, C. Cao, L. Peng, S. Li, D. Zhai, W. Song, *Nanoscale* **2017**, 9, 13538.
- [21] P. Liu, L. Wang, Y. Yang, Y. Qu, L.-J. Ming, *Dyes Pigm.* **2021**, 188, 109214.
- [22] L. Wang, Y.-X. Yang, X. Shi, S. Mignani, A.-M. Caminade, J.-P. Majoral, *J. Mater. Chem. B* **2018**, 6, 884.
- [23] M. Craven, R. Yahya, E. Kozhevnikova, R. Boomishankar, C. M. Robertson, A. Steiner, I. Kozhevnikov, *Chem. Commun.* **2013**, 49, 349.
- [24] M. Dutkiewicz, M. Przybylak, R. Januszewski, H. Maciejewski, *Polym. Degrad. Stab.* **2018**, 148, 10.
- [25] A. Steiner, *Polyphosphazenes Biomed. Appl.* **2009**, 411.
- [26] J. F. Bickley, R. Bonar-Law, G. T. Lawson, P. I. Richards, F. Rivals, A. Steiner, S. Zacchini, *Dalton Trans.* **2003**, 32, 1235.
- [27] M. A. Benson, S. Zacchini, R. Boomishankar, Y. Chan, A. Steiner, *Inorg. Chem.* **2007**, 46, 7097.
- [28] A. Uslu, S. Yeşilot, *Dalton Trans.* **2021**, 50, 2324.
- [29] H. Lu, A. Gruverman, *Organic Ferroelectric Materials and Applications*, Elsevier, NY **2022**.
- [30] H.-Y. Zhang, X.-G. Chen, Y.-Y. Tang, W.-Q. Liao, F.-F. Di, X. Mu, H. Peng, R.-G. Xiong, *Chem. Soc. Rev.* **2021**, 50, 8248.
- [31] C. R. Huang, Y. Li, Y. Xie, Y. Du, H. Peng, Y. L. Zeng, J. C. Liu, R. G. Xiong, *Angew. Chem., Int. Ed.* **2021**, 60, 16668.
- [32] T. Vijayakanth, D. J. Liptrot, E. Gazit, R. Boomishankar, C. R. Bowen, *Adv. Funct. Mater.* **2022**, 32, 2109492.
- [33] K. McKenna, A. Shluger, V. Iglesias, M. Porti, M. Nafria, M. Lanza, G. Bersuker, *Microelectron. Eng.* **2011**, 88, 1272.
- [34] K. Y. Lee, D. Kim, J. H. Lee, T. Y. Kim, M. K. Gupta, S. W. Kim, *Adv. Funct. Mater.* **2014**, 24, 37.
- [35] M. Arous, H. Hammami, M. Lagache, A. Kallel, *J. Non-Cryst. Solids* **2007**, 353, 4428.